Hindawi Publishing Corporation
Laser Chemistry
Volume 2006, Article ID 35373, 11 pages
doi:10.1155/2006/35373

Review Article

Optical Coherence Tomography for Artwork Diagnostics

Piotr Targowski, Michalina Góra, and Maciej Wojtkowski

Institute of Physics, Nicolaus Copernicus University, ul. Grudziądzka 5, 87 100 Toruń, Poland

Received 15 September 2006; Revised 8 December 2006; Accepted 15 December 2006

Recommended by Costas Fotakis

An overview of the optical coherence tomography (OCT) technique is given. Time domain, spectral and sweep source modalities are briefly described, and important physical parameters of the OCT instrument are discussed. Examples of the application of OCT to diagnosis of various art objects such as oil paintings on canvas (imaging of glaze and varnish layers), porcelain, faience, and parchment are presented. Applications to surface profilometry of painting on canvas are also discussed.

Copyright © 2006 Piotr Targowski et al. This is an open access article distributed under the Creative Commons Attribution License, which permits unrestricted use, distribution, and reproduction in any medium, provided the original work is properly cited.

1. INTRODUCTION

For more than a century, since a year after their discovery by W. Roentgen in 1895, X-rays have been used for investigation of art objects [1]. Since then, this and other noninvasive methods for diagnosis of artwork structure and properties have been developing rapidly. Such methods generally fall into two categories: (a) those directly revealing structure, and (b) profilometric ones which provide a 3D surface profile of the object. This second approach may also lead to structural information such as location of cracks or detachments [2]. Analytical methods requiring the extraction of a sample of the material, and therefore in principle destructive, and limited as to choice of position and number of samples, are not considered further. Some other methods, such as laser induced breakdown spectroscopy (LIBS) [3, 4], Raman spectroscopy [4, 5] or, among more classical approaches, UV [6–8] and laser induced fluorescence (LIF) [9], and IR reflectography [10], are either limited to the object surface, or the information provided is integrated over the whole thickness of the object. In the latter case, structural information has to be obtained indirectly. X-ray radiography and neutron activation autoradiography [11] of paintings serve as examples in which such an indirect approach is taken. In both cases, the location of certain pigments in the picture may be revealed, and sometimes lead to the discovery of different, underlying images. However, assignment of the pigment to a certain paint layer has to be made by comparison with the visible image. Whilst routine tomographic methods like ultrasonography, X-radiography, electron paramagnetic resonance, and nuclear magnetic resonance have been successfully used for artwork diagnosis, the resolution of even highly developed modern instruments, usually designed for medical diagnosis, is not sufficient for detailed examination of certain objects of art, for example, paintings. A more detailed discussion of noninvasive testing is beyond the scope of this short review. However, despite the tremendous proliferation of many, very advanced diagnostic techniques, there is still a need for a fast, portable, easy-to-use, and simple-to-interpret, method of high resolution, noninvasive structural imaging. These requirements may, to some extent, be fulfilled by optical coherence tomography (OCT), since this method needs neither pretreatment of the object, nor special mounting conditions, such as an optical table. Modern medical OCT devices are suitably mobile, and achieve micrometre resolution.

OCT is a novel optical technique enabling cross-sectional imaging of the internal structure of semitransparent objects. This technique is based on interferometry of partially coherent light [12]. OCT has the great advantage of yielding high resolution cross-sectional images in a noncontact and noninvasive way, with very high sensitivity [13]. Because of these advantages, OCT is particularly suitable for medical applications, especially for investigating structures in the human eye, which is naturally transparent to visible and near-infrared light, and almost inaccessible by any other diagnostic instrumentation [14]. OCT has been under development over the last fifteen years, and has successfully been commercialized for ophthalmological use.

In all OCT devices, the interference phenomenon is used to reveal the axial structure of the object analyzed, that is,

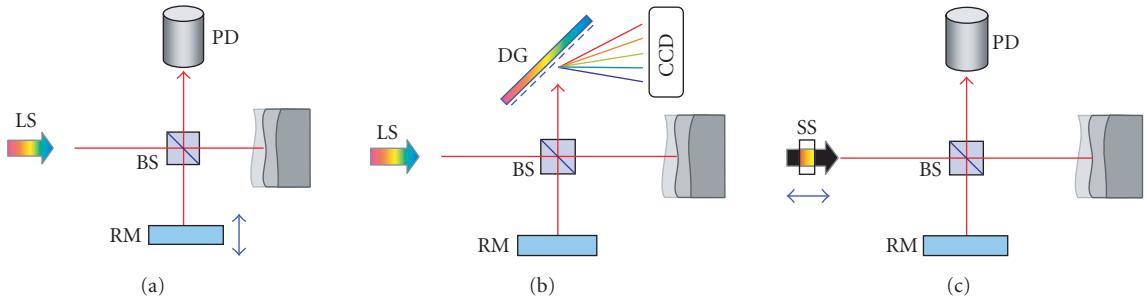

Figure 1: Consecutive generations of OCT devices: (a) time domain OCT, (b) spectral OCT, (c) sweep source OCT. Legend: LS—broadband light source, BS—beam splitter, PD—photodiode, DG—diffraction grating, RM—reference mirror, SS—sweep light source.

the distribution of back-scattering or back-reflecting points along the penetrating light beam. In order to obtain an interference fringe pattern carrying information about the axial structure of the object, the input light beam is split into two beams in the interferometer setup. The object is placed in the direct-beam arm of the interferometer, while the reference beam in the other arm is reflected back by the reference mirror (see Figure 1). The probing light, which is back-scattered or reflected by the internal structures of the object, is brought to interference with the reflected light returning from the reference arm. Since all light sources used for OCT have very short coherence times, this interference enables precise measurement of the optical path difference between the reference mirror position and the locations of the scattering or reflecting centres within the object. The basis of the technique is somewhat similar to that of radar, but the wavelengths utilized are much shorter and provide resolution in the micrometre range. In the next section, a simple basic description of the OCT technique is presented. A more comprehensive review may be found in many papers, for example, the article of Tomlins and Wang [15].

2. THE OCT INSTRUMENT

The majority of OCT instruments at present utilize optical fibres. However, for simplicity of description, the optical arrangements presented in this section are depicted in Figure 1 with bulk optics. They should therefore not be considered as experimental layouts, but rather as illustrating the physical ideas.

2.1. *The first generation: time domain OCT*

Time domain OCT (TdOCT, Figure 1(a)) was introduced [12] in 1991. In its most widespread version, it comprises a light source (LS) emitting light of high spatial and low temporal coherence, and a Michelson interferometer which divides the light beam and directs it into two orthogonal arms. The direct arm (object arm) terminates at the object to be analyzed. It usually contains collimating optics enabling formation of a narrow beam which penetrates the object. In order to reconstruct two-dimensional cross-sectional images of the object, the beam is galvanometrically scanned across its surface. Light backscattered or reflected from the various structures returns to the interferometer and is brought to interference with light propagating in the orthogonal arm (reference arm) which is terminated with a mirror (RM). The reference mirror RM is scanned back and forth through the required depth of imaging. The interfering light is detected by a photodiode (PD) backed up with a bandpass filter tuned to the Doppler frequency, often called the "carrier frequency," which is related to the scanning speed of the reference mirror. This procedure helps to eliminate extraneous signals arising from background light.

When the optical path length of the reference arm and object arm are properly matched, an interference fringe signal appears. When partially coherent light is used, the change of reference mirror position away from the matched one causes a rapid decrease of fringe contrast. Assuming that the measured object contains more than one reflecting interface or scattering structure, the condition of matched optical path lengths of the interferometric arms will be fulfilled many times during the scan of the reference mirror. As a result, a set of interferometric signals will be detected as a function of the reference mirror position. This set corresponds with the axial distribution of scattering and reflecting interfaces within the object, and it is named, by analogy with ultrasound biomicroscopy, the A-scan. For the next scan of the reference mirror, the probing beam is shifted to an adjacent position and so on, to yield a set of consecutive A-scans. These A-scans are then combined into a single picture to form a cross-sectional image of the object, the B-scan.

A major advantage of the time domain OCT instrument is its simple basic design and essentially unlimited depth of imaging, which depends only on the range of movement of the reference mirror. However, this movement is simultaneously a major drawback. Despite very sophisticated construction, this movable part slows down the data acquisition process to no better than 200 A-scans/second, even in the most advanced systems [16].

Instruments based on this principle are available commercially for medical diagnostic purposes. The most popular is the Stratus OCT™ from Zeiss-Meditec (USA), designed for imaging of the human retina. This system is optimized for medical applications, and it cannot directly be used for imaging materials. Instruments dedicated to the anterior chamber

of the eye (Visante OCT™ from Zeiss-Meditec) and other medical purposes are available, though less popular, but are also suitable for this application.

2.2. The second generation: spectral OCT

The theoretical basis for spectral OCT (SOCT, also called spectral domain OCT, Figures 1(b) and 2) [17] was published only two years after that of time domain OCT, but due to technological limitations (in particular the lack of very fast imaging systems) it did not generate much interest for a number of years. However, advances in high-speed and high-sensitivity CCD technology eventually enabled the development of spectral OCT instrumentation suitable for medical studies, and the first *in-vivo* images of the eye [18] were published in 2002. More recently, improvements in this technology have been developing rapidly [19–22].

In SOCT systems (Figure 1(b)), the single light intensity detector (PD in Figure 1(a)) is replaced by a spectrograph comprising a diffraction grating (DG) and fast camera (CCD). The spectrum of the light source registered by this camera is modulated by interference fringes of frequency corresponding to the position of the reflective or scattering layer in the object: the deeper the layer, the higher the modulation frequency. In contrast to time domain OCT, information about the entire axial structure of the object analyzed is collected simultaneously in one "shot" of the CCD camera. This information is encoded in the frequency signal. It is stored and subsequently decoded by numerical (reverse) Fourier transformation (FFT), conveniently performed on a personal computer.

The major advantage of SOCT is the lack of movable parts in the reference arm of the interferometer. Here, change of optical delay in the time domain is replaced by analysis of interference signals in the frequency domain. Due to this modification, the data collection period is significantly decreased, and acquisition speeds of up to 25,000 A-scans/second are currently attainable. The high speed of the SOCT system, which is very important for medical imaging, may also play a significant role in the application of OCT to art objects. For instance, it allows the multislice data collection necessary for 3D imaging of whole varnish layers and the subsequent analysis of varnish thickness. Spectral OCT also exhibits higher sensitivity than time domain OCT.

The main disadvantages of SOCT are directly related to the limitations of the CCD camera: the spectral sensitivity currently available restricts the wavelength range, and the number of pixels limits the range of modulation frequencies that can be recorded. In consequence, the depth of imaging of the system is limited. However, it is still usually not less than 1 mm, which is sufficient for the majority of OCT applications to the imaging of art objects. Another disadvantage is that SOCT systems appear to be somewhat more sensitive than TdOCT to saturation by mirror reflections from the sample. In spite of these drawbacks, the recently developed short acquisition time and high resolution now offered by SOCT instruments are beginning to take over in the market of medical diagnostic tools. At present (December 2006), the most advanced, commercially available SOCT instruments, are the SOCT Copernicus from Optopol S.A. (Poland) and the RTVue from Optovue Corp. (USA).

2.3. The third generation: sweep source OCT

In sweep source OCT (SSOCT, Figure 1(c)), detection is again performed by a single photodiode (PD) but, as in spectral OCT, interference spectra are measured, in this case by changing the wavelengths of the monitoring light with time. This is accomplished by using a sweep source laser (SS) as the light source. This device enables a change of the wavelength generated over a range of up to 100 nm within a couple of microseconds [23–27]. As in SOCT, reverse Fourier transformation is utilized to recover the structure of the object. The major advantage of this emerging OCT technology is the similar high speed of data acquisition to SOCT, but without its drawbacks, that is, spectral limitations of the CCD camera, imaging depth limitations due to the limited number of pixels in CCD devices, and loss of sensitivity with depth, all inherent to SOCT. The price currently to be paid is that the light source is very expensive and so far still not reliable in operation, as well as it presently being available only for a limited range of wavelengths around 1300 nm. However, it is expected that the spectral range available will be expanded in the near future.

2.4. General considerations

The most important parameters of OCT systems for application to the imaging of art objects are axial and lateral resolution, range of axial imaging, central wavelength of probing light, sensitivity, and acquisition speed.

Similarly to confocal microscopy, the lateral resolution is related to the focused spot size Δx of the probing beam. This depends on the magnification and numerical aperture of the optics used in the object arm, and can be expressed in terms of the focal length of the lens f forming the probing beam, and the original beam diameter d. It is estimated from the central wavelength λ_{centre} and the refractive index (n_R) of the medium examined:

$$\Delta x = \frac{1}{n_R}\frac{4\lambda_{\text{centre}}}{\pi}\left(\frac{f}{d}\right). \tag{1}$$

The axial resolution (Δz) depends on the spectral properties of the probing light through its central wavelength λ_{centre} and spectral span $\Delta\lambda_{\text{FWHM}}$:

$$\Delta z = \frac{1}{n_R}\frac{2\ln 2}{\pi}\frac{\lambda^2_{\text{centre}}}{\Delta\lambda_{\text{FWHM}}}. \tag{2}$$

It should be emphasized that (2) is derived with some idealized assumptions such as Gaussian shape for the spectrum. This condition is not fulfilled for real light sources. Also, in real systems, dispersion in the material examined causes additional broadening of the signal. This effect may be compensated both optically and numerically, but only to a certain extent. Numbers obtained from (2) should therefore serve rather as lower estimates for expected values.

Table 1: Examples of light sources used for OCT and available optical properties of the OCT system. In all cases, common values of $n_R = 1.4$ and $f/d = 12$ were used in (1)–(3).

The light source	λ_{centre} [nm]	$\Delta\lambda_{\text{FWHM}}$ [nm]	Δz [μm]	Δx [μm]	DOF [μm]
SLD	830	19	11.5	9	220
SLD (broadband)	830	50	4.4	9	220
SLD	1300	50	10.6	14	340
SLD	1560	100	7.6	17	410
The Broadlighter^{TM}	830	70	3.1	9	220
Integral OCT^{TM}	800	120	1.7	9	210
Femtosecond Ti: sapphire laser	850	144	1.6	9	220

The range of axial imaging is determined by various factors. Firstly, in all SOCT systems and the majority of TdOCT systems, it is limited by the depth of focus (DOF) of the probing beam

$$\text{DOF} = 2\Delta x\left(\frac{f}{d}\right). \tag{3}$$

This limitation may be overcome in TdOCT by using a focusing lens which moves simultaneously with the reference mirror to keep the coherence gate always in focus. In such a system, the imaging range may be extended to even as much as a few centimetres. In SOCT instruments, the imaging range is additionally and predominantly limited by the number of pixels of the CCD camera, which determines the maximum detectable frequency of spectral fringes. In practice, SOCT systems have an imaging range of about 2 mm.

The major factor determining the properties of any OCT system is the light source. To ensure high sensitivity, it has to emit highly spatially coherent light. Simultaneously, according to (2), it should have as broad a spectrum as possible. The most popular light sources fulfilling these conditions are semiconductor superluminescent diodes (SLD). Incandescent white light sources and specially designed lasers are also used for OCT applications [28]. Recent developments in the field of semiconductor lasers have yielded novel and cost effective spectrally broadband light sources built up from systems of SLDs, coupled together with optical fibres into a single source (the Broadlighter^{TM}).

Available light sources are limited to the near infrared range, namely, from 700 nm to 1500 nm. The exact choice of the central wavelength depends on the prospective application, and is mostly determined by the absorption properties of the medium under investigation, though the expected resolution must also be taken into account. In Table 1, common examples of light sources used in OCT, and the resulting system properties, are listed.

As can be seen from (2) and Table 1, the axial resolution deteriorates quickly with increasing central wavelength. This conclusion is important for the application to stratigraphy of paintings, because many pigments become transparent at longer wavelengths.

The sensitivity of the OCT instrument is a particularly important factor in nonprofilometric applications. It is defined as the reflectivity of the sample corresponding to the smallest signal which can be detected by the OCT system. The main source of noise in OCT devices is shot noise [22]. Assuming shot-noise-limited detection, the sensitivity of TdOCT instruments depends on the product of optical power (P_0) and exposure time (T_{ex}):

$$\text{Sensitivity}_{\text{TdOCT}} \propto T_{\text{ex}} \cdot P_0. \tag{4}$$

As compared with time domain OCT, SOCT systems have inherently higher sensitivity. This is due to the fact that SOCT enables simultaneous detection by the multipixel device (the CCD camera), and the integration time is effectively extended compared with that in TdOCT. The noise is therefore averaged out more effectively, the sensitivity being improved by a factor of N/2 (Nyqvist limit)

$$\text{Sensitivity}_{\text{SOCT}} \propto \frac{N}{2}\text{Sensitivity}_{\text{TdOCT}}, \tag{5}$$

where N is the number of pixels of the CCD camera used in the detector train.

The final operational parameter is the acquisition speed. As mentioned previously, SOCT systems are up to 100 times faster than TdOCT ones, which allows real-time monitoring of certain processes and the collection of volume (3D) data.

2.5. Exemplary hardware solutions

By choosing from time domain, spectral, and sweep source OCT systems, and by adopting a suitable light source (Table 1), one may assemble a system best fitting the prospective application. Some examples of such devices are described in detail elsewhere in this volume: the medium-resolution time-domain instrument, built in the Medical University in Vienna, and additionally capable of birefringence measurements, is depicted by Góra et al. [29]. Another bulk optics system of similar resolution, but of the spectral type, is described in the article concerning varnish ablation monitoring with OCT [30]. The latter instrument was utilized also for obtaining the stratigraphic images shown in Figures 3–5 and 8. To provide an example of a fibre optics device of slightly higher resolution, one of the instruments built in our laboratory for medical imaging, but also used for art diagnostics (see [31] and Figures 6 and 7), will be described below. It utilizes a Broadlighter^{TM} (from Superlum, Russia) as a light source, and so may be considered a high-resolution system. This broadband light source LS (Figure 2) comprises two coupled superluminescent diode modules with slightly

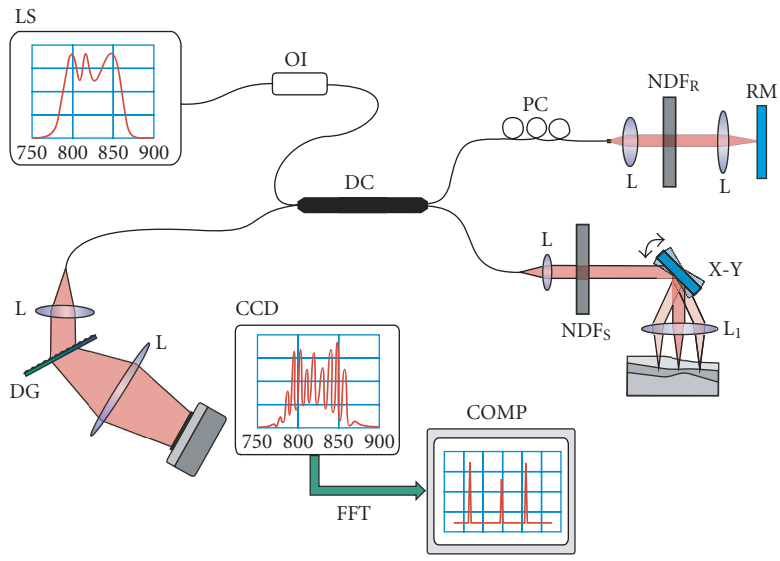

Figure 2: The setup of a spectral OCT instrument. Legend: LS—light source, OI—optical isolator, DC—directional coupler, PC—polarization controller, NDF—neutral density filters, RM—reference mirror, X-Y—scanners, L—lenses, DG—diffraction grating, CCD—linear CCD camera, COMP—personal computer where data processing (primarily fast Fourier transformation) is performed.

shifted central wavelengths. As a result, light of 5 mW output power and high spatial but low temporal coherence, with a spectrum (see insert in Figure 2) at $\lambda_{centre} = 823$ nm and $\Delta\lambda_{FWHM} = 74$ nm, is launched into one of the single mode fibres of the 50 : 50 fibre coupler DC through an optical isolator OI. The optical isolator protects the light source from light back-reflected from the elements of the interferometer, to which it is very sensitive. In the coupler, the incoming light is split into two arms: the reference and object arms. The reference arm consists of a polarization controller PC, a collimator, and an open-air delay line with a reflective mirror RM held in a fixed position. The object arm comprises a collimator, transversal scanners X-Y, and lenses L and L_1. The lens L_1 is placed between the scanner and the object in such a manner that the separation between lens and object, and between the pivot point of the scanner and the lens, are equal to the focal length of the lens. This optics produces a narrow beam of light which penetrates the object, and scatters from elements of its structure. Part of the scattered light is collected by the same optics L_1 and L, and directed back to the coupler DC. It then interferes with the light returning from the reference arm, and this signal is directed into a custom-designed spectrometer. The main part of the detector is a volume phase holographic grating DG with 1200 lines/mm. An achromatic lens L ($f = 150$ mm) focuses the spectrum on a 12-bit line scan CCD camera. The spectral fringe patterns registered by this detector are then transferred to a personal computer COMP. The resulting signal, that is, the spectral fringe pattern, is Fourier-transformed into a single line (A-scan) of a cross-sectional image. In order to obtain either a 2D slice (B-scan, Figure 3(a), e.g.) or a 3D volume tomogram, the beam is scanned transversely by galvanometric scanners X-Y.

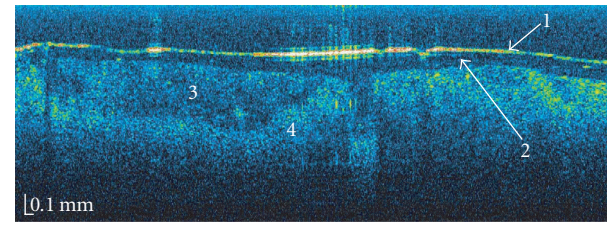

(a)

(b)

(c)

Figure 3: An example of OCT stratigraphy (a) of the oil painting on canvas, (b) the *Portrait of Sir James Wylie*. The tomogram (a) shows the cross-section taken at the place indicated by the vertical bar in the macro-photograph (c). Paintings by courtesy of the Institute for the Study, Restoration, and Conservation of Cultural Heritage, N. Copernicus University, Poland.

The system is shot-noise-limited (the intensity of light in the reference arm of the interferometer is controlled by the neutral density filter NDF) and the overall sensitivity is 90 dB. The exposure time per A-scan is 50 μs, so that a single 2D slice (composed usually of 2000 to 5000 A-scans) is collected in a fraction of a second. In addition to straightforward FFT processing, subtraction of noninterference background, spectral shaping [32], and numerical dispersion correction are carried out [33].

3. OCT DIAGNOSTICS OF MUSEUM OBJECTS

Over the last four years, an increasing number of applications of OCT to various aspects of art diagnostics have been reported. Both time-domain and spectral OCT modalities have been utilized. In this section, an overview of these applications will be given.

3.1. Stratigraphic applications

Since OCT examination is nondestructive, this method of analyzing the internal structure of such delicate objects as paintings on canvas is an obvious application, and has been quite widely explored. The major limitation is the restricted transparency of pigments, even in the infrared. Systematic studies [34] of 47 pigments showed that about a third of them exhibited good transparency at 1500 nm, and about a fifth of them at 820 nm. About another one eighth could be examined in thin layers at either wavelengths. Especially good results are obtained for red pigments (see Figure 3) [35].

The SOCT image (a B-scan) is shown in false colours: white and red colours indicate high scattering of penetrating light, while blue indicates low scattering. The light (λ_{centre} = 830 nm) penetrates the object from the top, and the first structure evident in the image is the surface of the painting (1). The varnish layer (2) does not scatter light, and is visible as a dark strip. Below this, the semitransparent glaze layers (3) and the absorbing paint layer (4) are visible.

Due to its ability to collect a large quantity of data in a short time, spectral OCT is especially well suited for obtaining volume information. In this case, a set of consecutive, adjacent B-scans is collected to cover a desired area of the object's surface. This data may be used to create flow-through films (see supplementary AVI file available at doi 10.1155/2006/35373).

It must be emphasized that, since many pigments are not transparent enough to permit clear structural imaging, this application of OCT is at present restricted to selected areas of paintings. Since the transparency of many pigments increases with the wavelength of penetrating light, significant progress may be expected from the application of longer wavelengths, in the range of 1.5–2.5 μm. However, to maintain reasonable axial resolution, these sources are required to have extremely broad spectra. Together, these conditions point to sweep source OCT as the most promising technique of the future.

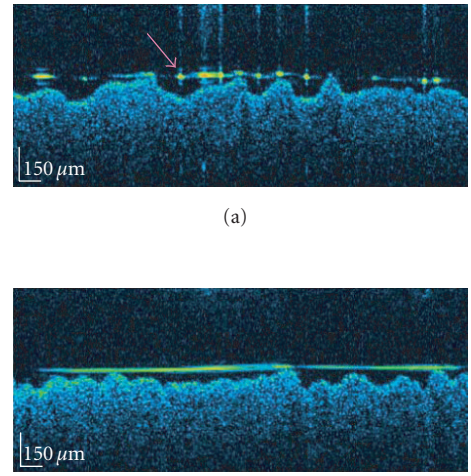

Figure 4: Contemporary layer of varnish: (a) acryl (Talens 114) of high molecular weight—local mirror reflections are seen as bright dots (arrow), (b) ketone (Talens 002) of low molecular weight—in this case the varnish surface is practically mirror flat.

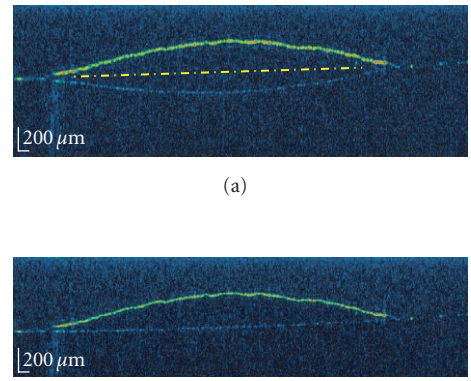

Figure 5: A drop of Rembrandt Varnish Matt from Talens (the Netherlands) on a glass substrate. (a) An uncorrected image. The originally flat glass plate appears concave in the cross-section due to refraction. (b) Image corrected by ray tracing procedure with n_R(varnish) = 1.55.

3.2. Varnish layer analysis

Limitations connected with pigment transparency are not of concern in imaging the varnish layer (Figures 4 and 5(a), see also Figure 3(a), layer 2). Although this layer is particularly easy to image, instruments with high axial resolution are nevertheless highly desirable. Direct comparison with a microscope cross-sectional image corresponding to the area analyzed with OCT shows perfect agreement of the results obtained by means of these two different methods [36]. High resolution OCT also permits the distinguishing of old and new varnish layers [37].

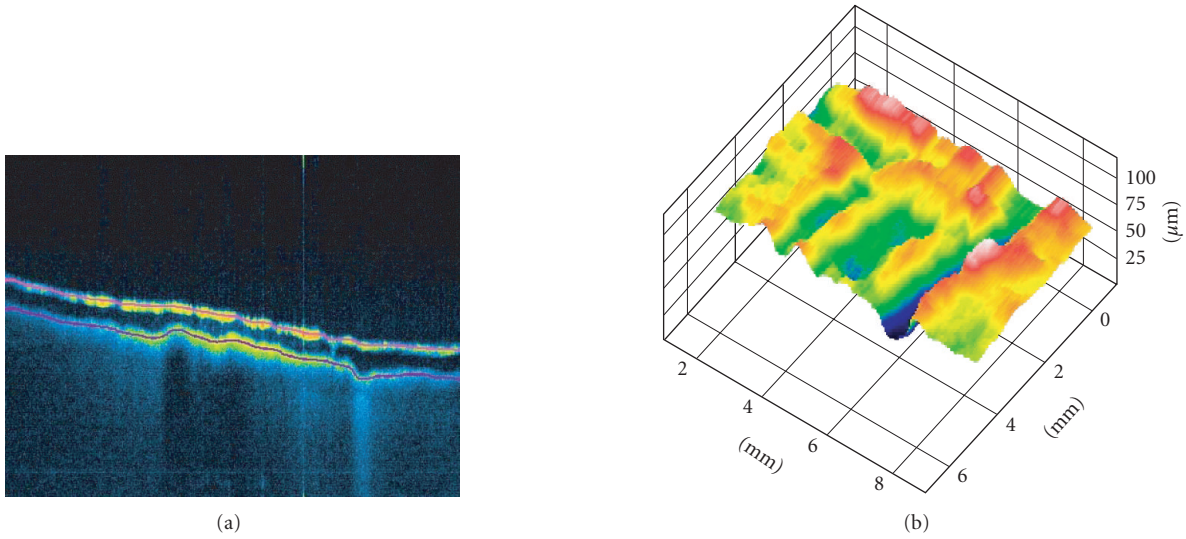

(a) (b)

Figure 6: (a) An OCT tomogram (B-scan) of a varnish layer over a nontransparent paint layer. Red lines denote the recognized interfaces: air-varnish and varnish-paint layer. (b) Varnish thickness map obtained by consecutive collection of 55 parallel OCT B-scans.

When a glossy varnish is imaged, mirror reflections from its surface become a significant difficulty (because of possible saturation of the detector). However, these reflections are a more significant problem in the imaging of fresh, contemporary layers. For historical varnishes, the surface is much less glossy, and tilting the picture slightly is usually enough to overcome the problem. Despite the above difficulty, reflections from the varnish surface also may serve as a measure of its roughness. Preliminary studies of Liang et al. [38] show that the surface of the acrylic varnish Paraloid B72 becomes less smooth and starts to follow the roughness of the substrate as it dries. They consider this as a convenient way of monitoring the wetting and drying process of paint and varnish layers.

In addition to the point raised above, this ability of acrylic varnish to reproduce the surface roughness of the paint layer is linked to the influence of varnish properties on the appearance of paintings. According to de la Rie [39], the varnish determines the final appearance of a picture in two ways: through its refractive index and through the roughness of its dried surface. It was shown that varnishes of high molecular weight (and thus of high viscosity), like modern acrylic media, reproduce the roughness of the surface of the paint layer. This effect, obtained in our laboratory with acrylic Talens 114 varnish (Paraloid B67), is presented in Figure 4(a). On the other hand, a varnish of low molecular weight, ketone Talens 002 (Figure 4(b)), levels the surface of the painting, which is much smoother after the varnish has dried—the mirror reflection is more homogeneous [35]. Historical varnishes composed of natural resins (e.g., dammar and mastic) also have low molecular weight and low viscosity in their liquid form. Consequently, the dried surface is mirror flat, which eliminates scattering of white light and thus increase the colour saturation.

Images of the varnish layer may be also utilized for a convenient measurement of its thickness. However, one must remember that the distances measured are optical and must be corrected to geometrical distances by dividing by the refractive index of the varnish. This effect is visible in Figure 5, as an artificial bending of the glass substrate. There are procedures available to correct images for this effect, if necessary. However, if layers are reasonably flat, simple vertical scale recalculation is sufficient.

If the varnish layer is well defined (compare Figure 3(a) with Figure 4(a)), automatic recognition of both air-varnish and varnish-paint layer interfaces is possible. An example is seen in Figure 6(a) (red lines). If such a procedure is applied to a set of parallel images, the varnish thickness map may be generated (see Figure 6(b)) [31].

An emerging, potentially important, application of imaging varnish layers with OCT is the use of OCT tomography to control the laser-induced varnish ablation process. In this case, OCT may be used to assay the ablation conditions, and to monitor the ablation process *in-situ* [30], the faster SOCT being particularly appropriate to the latter case.

3.3. Other structural analysis

One of the first applications of OCT to investigate the structure of cultural heritage artefacts was the imaging of glaze layers, on a porcelain cup and on a faience plate [40, 41]. OCT tomograms made in the same conditions and with the same instrument clearly show a thicker, less-scattering glaze layer on the porcelain (see Figure 7).

A similar application concerned imaging the structure of archaic jade artefacts from the Qijia and Liangzhu cultures in China [42]. With the aid of TdOCT instrumentation ($\lambda_{\text{centre}} = 800\,\text{nm}$, $\Delta\lambda_{\text{FWHM}} = 50\,\text{nm}$, $\Delta z(\text{in jade}) = 3.5\,\mu\text{m}$,

Figure 7: Comparison between OCT tomograms of Japanese porcelain (a) and faience (b).

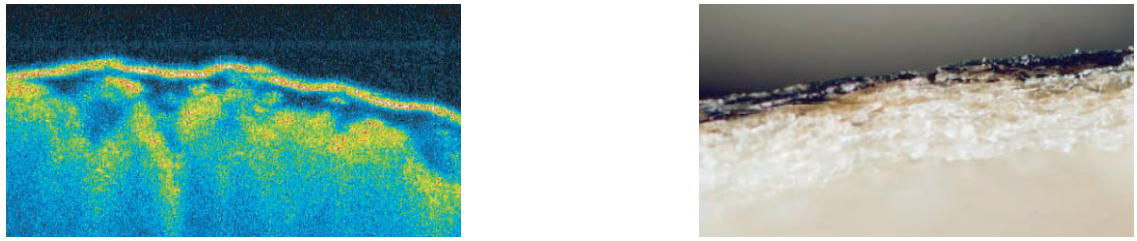

Figure 8: Comparison between an OCT tomogram (a) and a cut view taken in the same place ((b), photograph by Z. Rozłucka) of an artificially aged sample of parchment covered by iron gall ink.

and $\lambda_{\text{centre}} = 1240\,\text{nm}$, $\Delta\lambda_{\text{FWHM}} = 65\,\text{nm}$, $\Delta z\,(\text{in jade}) = 7.5\,\mu\text{m}$), the authors were able to distinguish between artificially treated (burned) and naturally whitened objects. This provides a valuable reference point for authenticating archaic jades.

A particularly interesting application of TdOCT has recently been proposed by Liang et al. [37]. They used an *en-face* modality of this technique to visualize underdrawings (preparatory drawings under the paint layer). In their system, a one layer (T-scan) perpendicular to the penetrating light is registered by scanning the probing beam over the investigated sample with an appropriate fixed position of the reference mirror. The mirror is then translated to the next position, and the whole procedure is repeated, and so on. Due to the narrow coherence gate (1), information from any given depth may be extracted with high contrast. When the position of the coherence gate is set to the depth at which underdrawings are expected, they are visible with a much better contrast than is available with classical methods, such as infrared imaging with a Vidicon or an InGaAs camera. Moreover, this technique allows, for the first time, the noninvasive determination of the layer in which the underdrawings appear.

Another potentially important application is in the imaging of parchment structure (see Figure 8). Preliminary studies have shown that it should be possible to use the OCT technique to trace structural deterioration caused by iron ink or other similar factors [29].

3.4. Profilometric applications

In these applications, OCT data is used to recover the first interface (i.e., that with air, see Figure 6(a), upper red line, e.g.). When the tracking procedure is applied to each slice in a set of 3D data, an elevation map of the surface may be recovered.

The first profilometric OCT experiment enabling analysis of the structure of a crack in a painting on canvas was performed in our laboratory [41, 43, 44]. The sample was placed in a climate chamber in which the temperature and relative humidity could be controlled. Surface maps were obtained before and after a significant humidity jump to assay the canvas response. The second experiment [45], also involving control in the climate chamber, was aimed at quantitative monitoring of whole canvas deformation. In this experiment, the position of a marker (a submillimetre spot of easy removable contrasting paint), placed at a chosen point on the canvas surface, was monitored simultaneously in 3 dimensions. Every 80 seconds, the area around a marker was scanned with the OCT probing beam. First, the IR reflectometric image of the surface was generated from the OCT data by integration over the whole depth of imaging. Then, the in-plane displacement of the marker was retrieved by numerical correlation with the previous image. Since the new in-plane position of the marker was established, its distance from the OCT head (the out-of-plane position) could be obtained from the OCT data by automatic recognition of the

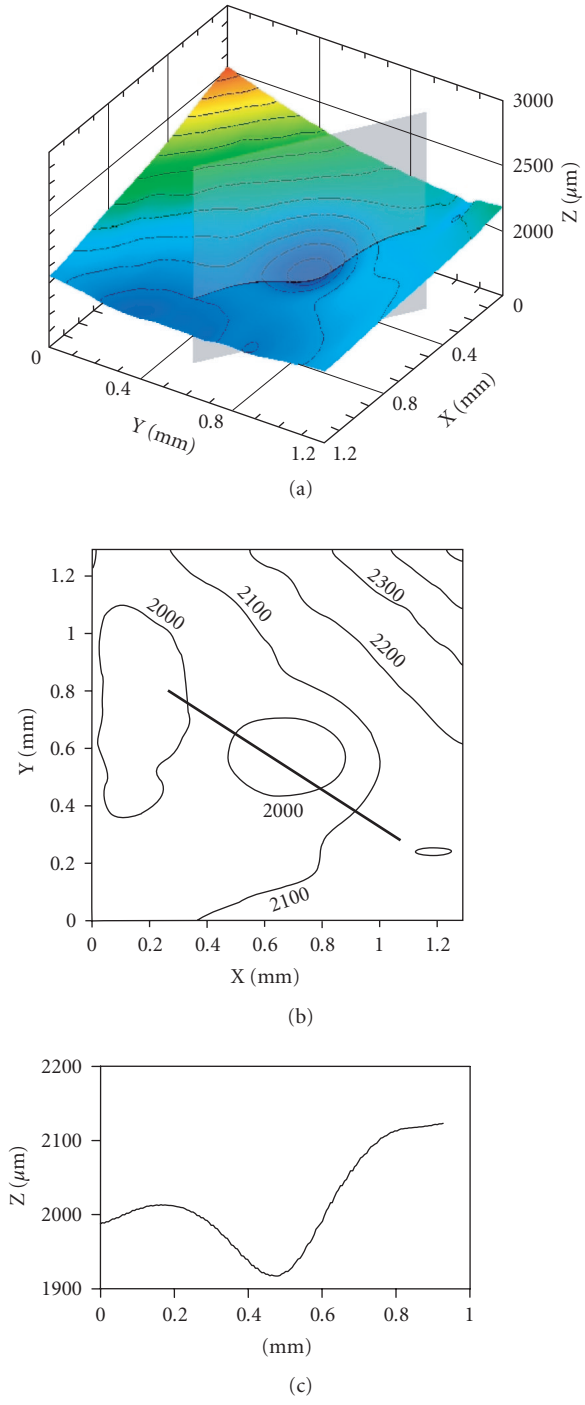

Figure 9: An example of alternative visualisations of the surface profile of an epoxy resin with the ablation crater visible; (a) orthographic surface view, (b) contour map—the heavy line indicates an arbitrary cross-section; (c) cross-sectional profile.

first scattering interface at the position of the marker. Tests show that the precision of marker position recognition is much better than the OCT image resolution of the same instrument (2 versus 8 μm for out-of-plane, and 8 versus 15 μm for in-plane displacements).

Surface profilometry may also prove useful in monitoring varnish removal processes. For example, in the case of laser ablation, the profile and depth of the ablation crater may be recovered. A detailed description and some results are given elsewhere [30]. In Figure 9, an example of our three presently available surface profile analyses is given. All these images were obtained from 3D OCT data comprising 200 parallel A-scans, each made up of 400 B-scans.

4. CONCLUSIONS

In conclusion of this short review of present and potential applications of OCT to diagnostics and documentation of art objects, it should be emphasized that at present it is still seeking for a subject best served by this analytic method. It seems that, for now, the role of the physicist is well defined. Further significant progress will only be possible if this method becomes adopted by art conservationists and analysts. Only experts directly involved in the investigation of the art object are able to ask questions of significant importance for an understanding of the structure and properties of the object examined. The physicist's further role is limited to modification of current instrumentation, and the design and implementation of new modalities, to provide a desirable diagnostic tools in response to this.

ACKNOWLEDGMENTS

This work was supported by Polish Ministry of Science Grant 2 H01E 025 25. Authors wish to thank Dr. Robert Dale for very valuable discussions.

REFERENCES

[1] C. F. Bridgman, "The future of radiography," *Bulletin of the American Institute for Conservation of Historic and Artistic Works*, vol. 14, no. 2, pp. 78–80, 1974.

[2] D. Ambrosini and D. Paoletti, "Holographic and speckle methods for the analysis of panel paintings. Developments since the early 1970s," *Reviews in Conservation*, vol. 5, pp. 38–48, 2004.

[3] D. Anglos, S. Couris, and C. Fotakis, "Laser diagnostics of painted artworks: laser-induced breakdown spectroscopy in pigment identification," *Applied Spectroscopy*, vol. 51, no. 7, pp. 1025–1030, 1997.

[4] M. Castillejo, M. Martín, D. Silva, et al., "Laser-induced breakdown spectroscopy and Raman microscopy for analysis of pigments in polychromes," *Journal of Cultural Heritage*, vol. 1, supplement 1, pp. S297–S302, 2000.

[5] P. Vandenabeele and L. Moens, " The application of Raman spectroscopy for the non-destructive analysis of art objects," in *Proceedings of the 15th World Conference on Nondestructive Testing*, Roma, Italy, October 2000, accessed 2006.

[6] E. R. de la Rie, "Fluorescence of paint and varnish layers—part I," *Studies in Conservation*, vol. 27, no. 1, pp. 1–7, 1982.

[7] E. R. de la Rie, "Fluorescence of paint and varnish layers—part II," *Studies in Conservation*, vol. 27, no. 2, pp. 65–69, 1982.

[8] E. R. de la Rie, "Fluorescence of paint and varnish layers—part III," *Studies in Conservation*, vol. 27, no. 3, pp. 102–108, 1982.

[9] D. Anglos, M. Solomidou, I. Zergioti, V. Zafiropulos, T. G. Papazoglou, and C. Fotakis, "Laser-induced fluorescence in artwork diagnostics: an application in pigment analysis," *Applied Spectroscopy*, vol. 50, no. 10, pp. 1331–1334, 1996.

[10] E. Walmsley, C. Metzger, J. K. Delaney, and C. Fletcher, "Improved visualization of underdrawings with solid-state detectors operating in the infrared," *Studies in Conservation*, vol. 39, no. 4, pp. 217–231, 1994.

[11] K. K. Taylor, M. J. Cotter, and E. V. Sayre, "Neutron activation autoradiography as a technique for conservation examination of paintings," *Bulletin of the American Institute for Conservation of Historic and Artistic Works*, vol. 15, no. 2, pp. 93–102, 1975.

[12] D. Huang, E. A. Swanson, C. P. Lin, et al., "Optical coherence tomography," *Science*, vol. 254, no. 5035, pp. 1178–1181, 1991.

[13] E. A. Swanson, J. A. Izatt, M. R. Hee, et al., "In vivo retinal imaging by optical coherence tomography," *Optics Letters*, vol. 18, no. 21, pp. 1864–1866, 1993.

[14] M. R. Hee, J. A. Izatt, E. A. Swanson, et al., "Optical coherence tomography of the human retina," *Archives of Ophthalmology*, vol. 113, no. 3, pp. 325–332, 1995.

[15] P. H. Tomlins and R. K. Wang, "Theory, developments and applications of optical coherence tomography," *Journal of Physics D: Applied Physics*, vol. 38, no. 15, pp. 2519–2535, 2005.

[16] A. M. Rollins, M. D. Kulkarni, S. Yazdanfar, R. Ung-Arunyawee, and J. A. Izatt, "In vivo video rate optical coherence tomography," *Optics Express*, vol. 3, no. 6, pp. 219–229, 1998.

[17] T. Dresel, G. Hausler, and H. Venzke, "Three-dimensional sensing of rough surfaces by coherence radar," *Applied Optics*, vol. 31, no. 7, pp. 919–925, 1992.

[18] M. Wojtkowski, R. Leitgeb, A. Kowalczyk, T. Bajraszewski, and A. F. Fercher, "In vivo human retinal imaging by Fourier domain optical coherence tomography," *Journal of Biomedical Optics*, vol. 7, no. 3, pp. 457–463, 2002.

[19] M. Wojtkowski, T. Bajraszewski, P. Targowski, and A. Kowalczyk, "Real-time in vivo imaging by high-speed spectral optical coherence tomography," *Optics Letters*, vol. 28, no. 19, pp. 1745–1747, 2003.

[20] M. Wojtkowski, V. J. Srinivasan, T. H. Ko, J. G. Fujimoto, A. Kowalczyk, and J. S. Duker, "Ultrahigh-resolution, high-speed, Fourier domain optical coherence tomography and methods for dispersion compensation," *Optics Express*, vol. 12, no. 11, pp. 2404–2422, 2004.

[21] R. A. Costa, M. Skaf, L. A. S. Melo Jr., et al., "Retinal assessment using optical coherence tomography," *Progress in Retinal and Eye Research*, vol. 25, no. 3, pp. 325–353, 2006.

[22] R. Leitgeb, C. K. Hitzenberger, and A. F. Fercher, "Performance of fourier domain vs. time domain optical coherence tomography," *Optics Express*, vol. 11, no. 8, pp. 889–894, 2003.

[23] S. H. Yun, C. Boudoux, M. C. Pierce, J. F. De Boer, G. J. Tearney, and B. E. Bouma, "Extended-cavity semiconductor wavelength-swept laser for biomedical imaging," *IEEE Photonics Technology Letters*, vol. 16, no. 1, pp. 293–295, 2004.

[24] S. H. Yun, G. J. Tearney, B. E. Bouma, B. H. Park, and J. F. De Boer, "High-speed spectral-domain optical coherence tomography at 1.3 μm wavelength," *Optics Express*, vol. 11, no. 26, pp. 3598–3604, 2003.

[25] R. Huber, M. Wojtkowski, K. Taira, J. G. Fujimoto, and K. Hsu, "Amplified, frequency swept lasers for frequency domain reflectometry and OCT imaging: design and scaling principles," *Optics Express*, vol. 13, no. 9, pp. 3513–3528, 2005.

[26] R. Huber, M. Wojtkowski, and J. G. Fujimoto, "Fourier Domain Mode Locking (FDML): a new laser operating regime and applications for optical coherence tomography," *Optics Express*, vol. 14, no. 8, pp. 3225–3237, 2006.

[27] R. Huber, M. Wojtkowski, J. G. Fujimoto, J. Y. Jiang, and A. E. Cable, "Three-dimensional and C-mode OCT imaging with a compact, frequency swept laser source at 1300 nm," *Optics Express*, vol. 13, no. 26, pp. 10523–10538, 2005.

[28] A. Dubois, L. Vabre, A.-C. Boccara, and E. Beaurepaire, "High-resolution full-field optical coherence tomography with a Linnik microscope," *Applied Optics*, vol. 41, no. 4, pp. 805–812, 2002.

[29] M. Góra, M. Pircher, E. Götzinger, et al., "Optical coherence tomography for examination of parchment degradation," *Laser Chemistry*, vol. 2006, Article ID 68679, 2006, 6 pages.

[30] M. Góra, P. Targowski, A. Rycyk, and J. Marczak, "Varnish ablation control by optical coherence tomography," *Laser Chemistry*, vol. 2006, Article ID 10647, 2006, 7 pages.

[31] I. Gorczyńska, M. Wojtkowski, M. Szkulmowski, et al., "Varnish thickness determination by spectral optical coherence tomography," in *Proceedings of the 6th International Congress on Lasers in the Conservation of Artworks (LACONA VI '05)*, J. Nimmrichter, W. Kautek, and M. Schreiner, Eds., Vienna, Austria, September 2006.

[32] M. Szkulmowski, M. Wojtkowski, P. Targowski, and A. Kowalczyk, "Spectral shaping and least square iterative deconvolution in spectral OCT," in *Coherence Domain Optical Methods and Optical Coherence Tomography in Biomedicine VIII*, vol. 5316 of *Proceedings of SPIE*, pp. 424–431, San Jose, Calif, USA, January 2004.

[33] B. Cense, N. A. Nassif, T. C. Chen, et al., "Ultrahigh-resolution high-speed retinal imaging using spectral-domain optical coherence tomography," *Optics Express*, vol. 12, no. 11, pp. 2435–2447, 2004.

[34] A. Szkulmowska, M. Góra, M. Targowska, et al., "The applicability of optical coherence tomography at 1.55 um to the examination of oil paintings," in *Proceedings of the 6th International Congress on Lasers in the Conservation of Artworks (LACONA VI '05)*, J. Nimmrichter, W. Kautek, and M. Schreiner, Eds., Vienna, Austria, September 2006.

[35] M. Targowska, "Pomiary konserwatorskie z wykorzystaniem metody tomografii optycznej -OCT (Examination of objects of art with optical coherence tomography)," M.S. thesis, Department of Conservation of Paintings and Polychrome Sculpture, Nicolaus Copernicus University, Toruń, Poland, 2006, B. Rouba Advisor.

[36] T. Arecchi, M. Bellini, C. Corsi, et al., "Optical coherence tomography for painting diagnostics," in *Optical Methods for Arts and Archaeology*, vol. 5857 of *Proceedings of SPIE*, pp. 278–282, Munich, Germany, June 2005.

[37] H. Liang, M. G. Cid, R. G. Cucu, et al., "En-face optical coherence tomography—a novel application of non-invasive imaging to art conservation," *Optics Express*, vol. 13, no. 16, pp. 6133–6144, 2005.

[38] H. Liang, M. G. Cid, R. G. Cucu, et al., "Optical coherence tomography: a non-invasive technique applied to conservation of paintings," in *Optical Methods for Arts and Archaeology*, vol. 5857 of *Proceedings of SPIE*, pp. 9 pages, Munich, Germany, June 2005.

[39] E. R. de la Rie, "The influence of varnishes on the appearance of paintings," *Studies in Conservation*, vol. 32, no. 1, pp. 1–13, 1987.

[40] P. Targowski, B. Rouba, M. Wojtkowski, I. Gorczyńska, and A. Kowalczyk, "Zastosowanie optycznej tomografii do nieinwazyjnego badania obiektów zabytkowych," in *Ars longa - vita brevis. Tradycyjne i nowoczesne metody badania dzieł sztuki. Materiały z sesji naukowej poświęconej pamięci profesora Z. Brochwicza*, J. Flik, Ed., pp. 121–129, Wydawnictwo UMK, Toruń, Poland, 2003.

[41] P. Targowski, B. Rouba, M. Wojtkowski, and A. Kowalczyk, "The application of optical coherence tomography to nondestructive examination of museum objects," *Studies in Conservation*, vol. 49, no. 2, pp. 107–114, 2004.

[42] M.-L. Yang, C.-W. Lu, I.-J. Hsu, and C. C. Yang, "The use of optical coherence tomography for monitoring the subsurface morphologies of archaic jades," *Archaeometry*, vol. 46, no. 2, pp. 171–182, 2004.

[43] T. Bajraszewski, I. Gorczyńska, B. Rouba, and P. Targowski, "Spectral domain optical coherence tomography as the profilometric tool for examination of the environmental influence on paintings on canvas," in *Proceedings of the 6th International Congress on Lasers in the Conservation of Artworks (LACONA VI '05)*, J. Nimmrichter, W. Kautek, and M. Schreiner, Eds., Vienna, Austria, September 2006.

[44] P. Targowski, T. Bajraszewski, I. Gorczyńska, et al., "Spectral optical coherence tomography for nondestructive examinations," submitted to *Optica Applicata*.

[45] P. Targowski, M. Góra, T. Bajraszewski, et al., "Optical coherence tomography for tracking canvas deformation," *Laser Chemistry*, vol. 2006, Article ID 93658, 2006, 8 pages.